Scattering for mixtures of hard spheres: Comparison of total scattering intensities with model

B. J. Anderson,[1] V. Gopalakrishnan,[1] S. Ramakrishnan,[2] and C. F. Zukoski[1,*]
[1]*Department of Chemical and Biomolecular Engineering, University of Illinois at Urbana-Champaign, Urbana, Illinois 61801, USA*
[2]*Department of Chemical and Biomedical Engineering, Florida A&M–Florida State University, Tallahassee, Florida 32310, USA*
(Received 18 October 2005; published 23 March 2006)

The angular dependence of the intensity of x-rays scattered from binary and ternary hard sphere mixtures is investigated and compared to the predictions of two scattering models. Mixture ratio and total volume fraction dependent effects are investigated for size ratios equal to 0.51 and 0.22. Comparisons of model predictions with experimental results indicate the significant impact of the role of particle size distributions in interpreting the angular dependence of the scattering at wave vectors probing density fluctuations intermediate between the sizes of the particles in the mixture.

DOI: 10.1103/PhysRevE.73.031407 PACS number(s): 82.70.Dd, 61.10.Eq

I. INTRODUCTION

The mechanics and thermodynamics of suspensions composed of colloidal particles with monomodal size distributions have seen extensive study. The prototypical model suspension is composed of single sized hard spheres. The development of experimental systems that are excellent approximations of hard spheres have greatly advanced our understanding of order-disorder phase transitions [1,2], glass formation [3–5], and volume fraction dependencies of transport properties [6–8]. Substantially less work has been carried out on mixtures of well-defined particles. Particle mixtures are important for gaining an understanding of industrial suspensions: cosmetics, ceramics, foods, and coatings. For these applications, there is a desire to understand how particles of different size pack and how the microstructure influences the material properties of the resulting suspension.

One type of intensely studied mixture is a two component particle-polymer mixture where an increasing concentration of polymer will induce a gel phase transition due to attractive depletion interactions between particles caused by an exclusion of the polymer from the region between the particles [9–14]. A more basic mixture is a two component system of hard spheres differing significantly in size. Based largely on expanding the understanding of depletion effects, there has been increased theoretical and experimental work done on binary mixtures over the past 15 years [15–24]. Research has focused on understanding the dependence of mixture microstructure [15–21] and rheological properties [22–24] on component volume fractions.

A suspension of monomodal hardcore particles of type 1 can be characterized by five variables: particle diameter d_1, standard deviation in size distribution σ_1, volume fraction φ_1, and strength and range of attraction ε_1 and κ_1, respectively. Introducing a second set of particles introduces a second five variables d_2, σ_2, φ_2, ε_2, and κ_2 plus cross terms characterizing the strength and range of the interaction between particles of different size, ε_{12} and κ_{12}. Due to the difficulties of exploring a 12-dimensional space, limited progress has been made in understanding the general properties of mixtures. Once again a natural starting point is mixtures of repulsive hard sphere particles where the variable space is reduced to $3n$ where n is the number of discrete size distribution and 3 represents the particle diameter, breadth of the size distribution, and volume fraction of each component. Even with hard spheres the variable space to explore is immense. In this paper, our goal is to explore the angular dependent scattering properties of suspensions containing mixtures of Brownian hard spheres and compare experimental results with model predictions. This goal is motivated by the need to use such models to analytically explore the effects of introducing different component populations on a suspension microstructure.

In the past, detailed studies of such systems have been attempted by contrast matching the scattering of one component to that of the solvent in order to mask its scattering effects [15,18]. In this way the scattering of a second component can be investigated in the context of the mixture. In principle, for a binary mixture of particles of sizes 1 and 2, one can measure the correlations between particle pairs 11, 22, and 12. Although conceptually straight forward, the development of index matched systems is not trivial. In particular, the particles must have different compositions in order to be matched by different solvents and this provides ample opportunity to question the nature of the interactions between the various particle pairs. Duits *et al.* [15] report scattering from mixtures where the individual components behave largely like hard spheres but where the structure of the mixed suspension suggests that there is an unexpected attraction between particles of different size. From the work of Duits *et al.* and other work where partial structure factors have been reported [16–18], we can conclude that hard sphere models used to calculate the partial structure factors are incomplete or that there are experimental difficulties in extracting partial structure factors with the solvent matching method. Here we study the microstructure of mixtures of hard spheres composed of the same material. As a result we report total intensity and do not extract partial structure factors.

*Author to whom correspondence should be addressed. Email address: czukoski@uiuc.edu

Several authors have derived mathematical models that address the angle and volume fraction dependence of scattering of multicomponent suspensions of hard spheres [25–29]. In one approach, Ashcroft and Langreth calculate microstructures using the Percus-Yevick (PY) closure [25]. They utilize solutions to the PY closure to extract partial structure factors (correlations between pairs 11, 22, and 12) for the calculation of total scattering from a binary mixture. König and Ashcroft have recently extended this approach by solving for the partial structure factors of a ternary mixture [26]. A second approach developed by Vrij and co-workers calculates total scattering without the extraction of partial structure factors [28]. In this approach, analytical solutions for the scattered intensity are calculated for any multicomponent mixture.

In this work we compare the predictions of these two approaches with scattering from suspensions of binary mixtures of hard spheres determined experimentally. Below, in Sec. II, we provide a background for predicting the scattering from suspensions containing mixtures of particles followed in Sec. III by a description of our experimental methods. Section IV contains a discussion of how the models are fit to the experimental data and conclusions are drawn in Sec. V. We find the scattered intensity to be very sensitive to particle size distributions at scattering vectors that probe density fluctuations intermediate between the modal particle sizes. We conclude that the angular dependence of the total intensity is best modeled through the method of Vrij. Our results show that this approach provides a near quantitative prediction of the angle and volume fraction dependencies of the total scattering from two different binary mixtures and a ternary mixture.

II. MODELS

A. Scattering intensity

The scattering intensity for any p-component mixture is given by the relation

$$I(q) = \sum_{i,j=1}^{p} f_i f_j \sqrt{n_i n_j P_i(q) P_j(q)} S_{ij}(q) + B. \tag{1}$$

The first term refers to the intensity of the sample, $I_s(q)$, where f_i are the scattering amplitudes at zero angle, n_i are the number densities, $P_i(q)$ are the form factors accounting for intraparticle scattering interference for particles of type i, and $S_{ij}(q)$ are the structure factors accounting for interparticle scattering interference between particles of type i and j. The second term refers to background scattering, B. Background scattering is subtracted off of the intensity by the scattering of a reference. The variable q is the scattering vector [For x-rays, $q=4\pi/\lambda \sin(\theta/2)$ where λ is the wavelength of incident x-rays and θ is the scattering angle]. For a binary mixture the scattering intensity of a sample is given by the sum of three terms,

$$I_s(q) = n_1 f_1^2 P_1(q) S_{11}(q) + n_2 f_2^2 P_2(q) S_{22}(q) + 2 f_1 f_2 \sqrt{n_1 n_2 P_1(q) P_2(q)} S_{12}(q). \tag{2}$$

The first term is the scattering for the larger particles; the second term is scattering for the smaller particles; and, the third term is cross scattering between large and small particles. From this point on, the sample scattering subscript will be dropped. $I(q)$ will refer only to scattering from the sample. The scattering amplitudes in x-ray scattering depend on the volume of the scatter $V_{s,i}$ and the electron scattering length density contrast $\Delta\rho_e$ between the scatter and the solvent.

$$f_i = V_{s,i} \Delta\rho_e. \tag{3}$$

The partial structure factors are given by

$$S_{ij}(q) = \delta_{ij} + H_{ij}(q) = \delta_{ij} + (n_i n_j)^{1/2} \int_0^\infty 4\pi r^2 h_{ij}(r) \frac{\sin(qr)}{(qr)} dr, \tag{4}$$

where δ_{ij} is the Kronecker delta, $H_{ij}(q)$ are the interparticle interference functions, and $h_{ij}(r)$ are the total correlation functions. The integration variable r is the radial distance between two particle centers. The interparticle interference functions are never dealt with directly and are instead related to the Fourier transform of the direct correlation functions, $C_{ij}(q)$, through the Ornstein-Zernike (OZ) equation given here for a multicomponent mixture:

$$[\mathbf{I} + \mathbf{H}(q)][\mathbf{I} - \mathbf{C}(q)] = \mathbf{I}. \tag{5}$$

Solutions for the direct correlation functions can be obtained by applying a closure relation that describes the particle interaction potentials.

B. Ashcroft/Langreth model

Ashcroft and Langreth use the PY closure to derive an exact solution for the direct correlation functions and partial structure factors for a binary hard sphere mixture [25]. The PY closure for a mixture relates the radial distribution function, $g_{ij}(r)$, to the direct correlation function, $c_{ij}(r)$.

$$g_{ij}(r)(e^{-\beta\varphi_{ij}(r)} - 1) = e^{-\beta\varphi_{ij}(r)} c_{ij}(r). \tag{6}$$

$\varphi_{ij}(r)$ are the pair potentials and β is $1/k_B T$ where k_B is the Boltzmann constant. The radial distribution functions are related to the total correlation functions by $h_{ij}(r)=g_{ij}(r)-1$. Previous to Ashcroft and Langreth, Lebowitz worked out relations for the direct correlation functions generalized to a multicomponent mixture in the PY closure [30]. For a binary mixture, the direct correlation functions are

$$\begin{aligned} -c_{11}(r) &= a_1 + b_1 + mr^3, \quad r < d_1 \\ -c_{22}(r) &= a_2 + b_2 + mr^3, \quad r < d_2 \\ -c_{12}(r) &= a_2, \; r < \tfrac{1}{2}(d_1 - d_2) \equiv \gamma \\ -c_{12}(r) &= a_2 + [bR^2 + 4m\gamma R^3 + mR^4]/r, \; \tfrac{1}{2}(d_1 - d_2) < r < \tfrac{1}{2}(d_1 + d_2), \end{aligned} \tag{7}$$

where $R=r-1/2(d_1-d_2)$. Values for the coefficients a_i, b_i, and m are given in Appendix A. Using the Lebowitz rela-

tions, Ashcroft and Langreth derived expressions for the partial structure factors for a binary mixture. By taking the Fourier transforms of the direct correlation functions and its relation to the interparticle interference function (see Appendix A), the partial structure factors are calculated directly from $C_{ij}(q)$ through the following relations:

$$S_{11}(q) = \frac{[1 - n_2 C_{22}(q)]}{[1 - n_1 C_{11}(q) - n_2 C_{22}(q) + n_1 n_2 C_{11}(q) C_{22}(q) - n_1 n_2 C_{12}^2(q)]},$$

$$S_{22}(q) = \frac{[1 - n_1 C_{11}(q)]}{[1 - n_1 C_{11}(q) - n_2 C_{22}(q) + n_1 n_2 C_{11}(q) C_{22}(q) - n_1 n_2 C_{12}^2(q)]},$$

$$S_{12}(q) = \frac{n_1 n_2 C_{12}(q)}{[1 - n_1 C_{11}(q) - n_2 C_{22}(q) + n_1 n_2 C_{11}(q) C_{22}(q) - n_1 n_2 C_{12}^2(q)]}. \quad (8)$$

These partial structure factors are derived for a monodisperse binary mixture and do not account for polydispersity.

The particle form factors $P_i(q)$ for spherical particles are given by

$$P_i(q) = \left(3 \frac{\sin(q d_i/2) - (q d_i/2)\cos(q d_i/2)}{(q d_i/2)^3} \right)^2. \quad (9)$$

One can account for modest polydispersity in particle size by calculating $P_i(q)$ for a size distribution, but assume $S(q)$ remains that for monodisperse particles. This is done here by employing a Gaussian diameter distribution to calculate an average form factor for a population of particles with mean diameter d_i, and standard deviation σ_i. The integration variable d is the variable diameter of a particle.

$$\bar{P}_i(q) = \frac{\int \frac{1}{\sqrt{2\pi\sigma_i^2}} e^{[-(d-d_i)^2/2\sigma_i^2]} d^6 P(q) dd}{\int \frac{1}{\sqrt{2\pi\sigma_i^2}} e^{[-(d-d_i)^2/2\sigma_i^2]} d^6 dd}. \quad (10)$$

Prediction of the total scattering intensity requires measurements of P_i by fitting with Eq. (10) to determine d_i and σ_i. The total scattering is calculated using Eq. (2) with knowledge of the component number densities and scattering amplitude. $\bar{P}_i$ is used in Eq. (2) and the S_{ij}'s are calculated assuming the particles of type i are monodisperse with diameters d_i.

C. Vrij model

Vrij and co-workers [28] use the matrix form of the OZ equation [Eq. (5)] to transform the scattering intensity equation for a mixture to one dependent on the Fourier transform of the direct correlation functions. The partial structure factors [Eq. (4)] may be written

$$S_{ij}(q) = \delta_{ij} + H_{ij}(q) = [\Delta(q)]^{-1} |\mathbf{I} - \mathbf{C}(q)|^{ji}, \quad (11)$$

where

$$\Delta(q) = |\delta_{ij} - C_{ij}(q)| \quad (12)$$

is the $p \times p$ determinant of the matrix $[\mathbf{I} - \mathbf{C}(q)]$ and $|\mathbf{I} - \mathbf{C}(q)|^{ji}$ is the cofactor of the element $\delta_{ji} - C_{ji}(q)$ of this determinant. By substituting Eq. (11) into Eq. (2), the scattering intensity becomes

$$I(q) = [-D_f(q)][\Delta(q)]^{-1}. \quad (13)$$

The quantity $D_f(q)$ is the determinant of a $(p+1) \times (p+1)$ matrix:

$$D_f(q) = \begin{vmatrix} 0 & f_j \sqrt{n_j P_j(q)} \\ f_i \sqrt{n_i P_i(q)} & \delta_{ij} - C_{ij}(q) \end{vmatrix}. \quad (14)$$

Baxter showed that when the $c_{ij}(r)$ have finite ranges and tend to zero beyond distances $r > (d_i + d_j)/2$, the $c_{ij}(r)$ can be truncated so that Fourier integrations are performed over a finite range [31]. This allows the matrix $[\mathbf{I} - \mathbf{C}(q)]$ to be factored into $Q_{ij}(q)$ functions that are simpler in form than $C_{ij}(q)$,

$$[\mathbf{I} - \mathbf{C}(q)] = \mathbf{Q}^T(-q)\mathbf{Q}(q), \quad (15)$$

where

$$Q_{ij}(q) = \delta_{ij} - 2\pi(\rho_i \rho_j)^{1/2} \int_{s_{ij}}^{d_{ij}} q_{ij}(r) e^{iqr} dr \quad (16)$$

with limits of integration $d_{ij} = (d_i + d_j)/2$ and $s_{ij} = (d_i - d_j)/2$. The functions $q_{ij}(r)$ are a recasting of the direct correlation functions. The matrix form of the OZ equation becomes

$$[\mathbf{I} + \mathbf{H}(q)][\mathbf{Q}^T(-q)\mathbf{Q}(q)] = \mathbf{I}. \quad (17)$$

The Baxter condition leading to the truncation of $c_{ij}(r)$ is satisfied with the PY closure and the resulting functions $q_{ij}(r)$ are of the form

$$q_{ij}(r) = \frac{a_i}{2}(r^2 - d_{ij}^2) + b_i(r - d_{ij}), \quad (18)$$

for $s_{ij} < r < d_{ij}$, where

$$a_i = (1 - \xi_3 + 3\xi_2 d_{ii})/(1 - \xi_3)^2, \tag{19}$$

$$b_i = -\tfrac{2}{3} d_{ii}^2 \xi_2/(1 - \xi_3)^2, \tag{20}$$

and

$$\xi_\nu = \frac{1}{6}\pi \sum_{i=1}^{p} n_i d_{ii}^\nu. \tag{21}$$

By the substitution of Baxter's form of the OZ equation, expressions for the determinants $D_f(q)$ and $\Delta(q)$ can be cast in terms of ξ_ν (Appendix B). The total scattering intensity is calculated from Eq. (13). The interested reader should consult Vrij and co-workers [28,29] for a more detailed derivation and discussion of this approach.

In using the Vrij model, a Gaussian distribution was employed to account for the effects of polydispersity on the scattered intensity. A total number density distribution function was constructed as the sum of the distributions for each component:

$$n(d) = N \sum_{i=1}^{p} \frac{x_i}{\sqrt{2\pi\sigma_i^2}} \exp\left[\frac{-(d - d_i)^2}{2\sigma_i^2}\right]. \tag{22}$$

In the expression above, N is a normalization constant, x_i are the number fractions, and d_i and σ_i are the mean diameter and the standard deviation of the ith component. All summations over d were thus changed to integrations upon implementation of the total number density distribution.

D. Comparison of model predictions

The Ashcroft/Langreth (A/L) and Vrij (V) models depend on three parameters per component: d_i, σ_i, and φ_i. We are interested in understanding how these parameters alter scattering predictions within each model. Predictions of $I(q)$ for a two component mixture within each model are compared where each parameter is varied systematically (Figs. 1–3). At a first glance, we noticed that both models make similar predictions for low q ($q < 2\pi/d_1$) and high q ($q < 2\pi/d_2$) but differ significantly when probing intermediate q ($2\pi/d_1 < q < 2\pi/d_2$), length scales between the average sizes of the two components. This difference is discussed below.

In Fig. 1, predictions of $I(q)$ as a function of qd_1 where d_1 is the larger particle diameter assess the effect of varying the particle size ratio, $\alpha = d_2/d_1$. In Fig. 1(a) we show predictions of the A/L model and in Fig. 1(b) we show predictions of the V model. In both cases we have specialized the calculation for essentially monodisperse suspensions ($\sigma_1 = \sigma_2 = 0.05$) and $\varphi_1 = \varphi_2 = 0.2$. As α increases we see systematic suppression in $I(0)$ while the magnitude of the second peak (at $qd_1 \approx 11$) increases. At higher q, the details of $I(q)$ are complex functions of α for both models.

The effect of polydispersity is explored in Fig. 2 where we compare $I(q)$ with $\varphi_1 = \varphi_2 = 0.2$ and $\alpha = 0.25$ for different values of $\sigma = \sigma_1 = \sigma_2$. We show four curves, $\sigma = 0.001$ [Fig. 2(a)] and $\sigma = 0.1$ [Fig. 2(b)] in both models. When $\sigma = 0.001$, the two models show excellent agreement at high and low q. As we raise the polydispersity, slight differences

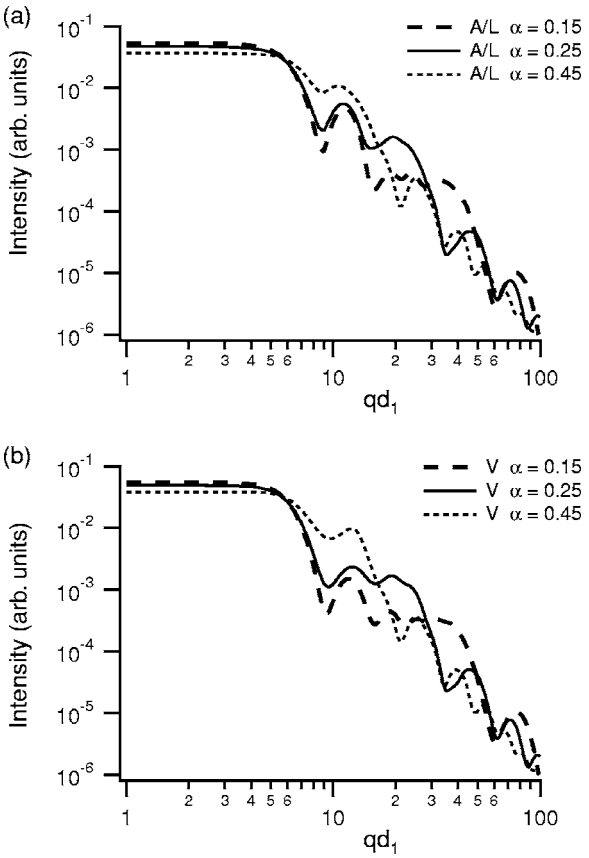

FIG. 1. Scattered intensity as a function of qd_1 holding constant $\varphi_1 = \varphi_2 = 0.2$ and $\sigma_i = 0.05$ while varying size ratio $\alpha = d_2/d_1$ as predicted in (a) the A/L model and (b) the V model.

in $I(q)$ emerge in the high and low q limits. Scattering peaks show a slight spreading in the V model. It is also apparent at high and low q that the scattered intensity in the V model is shifted up compared to Fig. 2(a) where predictions superimposed. These subtle differences can be attributed to the more complete inclusion of the effect of polydispersity in the scattering predictions of the V model, while polydispersity is only included in $P(q)$ in the A/L model. Calculations in the A/L model become unwieldy to include the effect of polydispersity in the partial structure factors. Vrij does not calculate the component average form factors or partial structure factors directly, but uses the matrix form of the Ornstein-Zernike equation and Baxter's approximation of the direct correlation functions to derive one scattering intensity equation for any multicomponent suspension once the total number density distribution is known. This simplifies the scattering equation and includes the total effect of polydispersity.

Polydispersity, however, does not explain the different scattering predictions at intermediate q. The different predictions for scattering around the second peak are unaltered as polydispersity is varied. The fact that the two models do not superimpose as $\sigma \to 0$ shows that polydispersity does not explain the different predictions for $2\pi/d_1 < q < 2\pi/d_2$.

We are also interested in how the models predict changes in scattering as a second component is added to the suspension. In Fig. 3 we show model predictions as a second component φ_2 is added to a single component suspension where

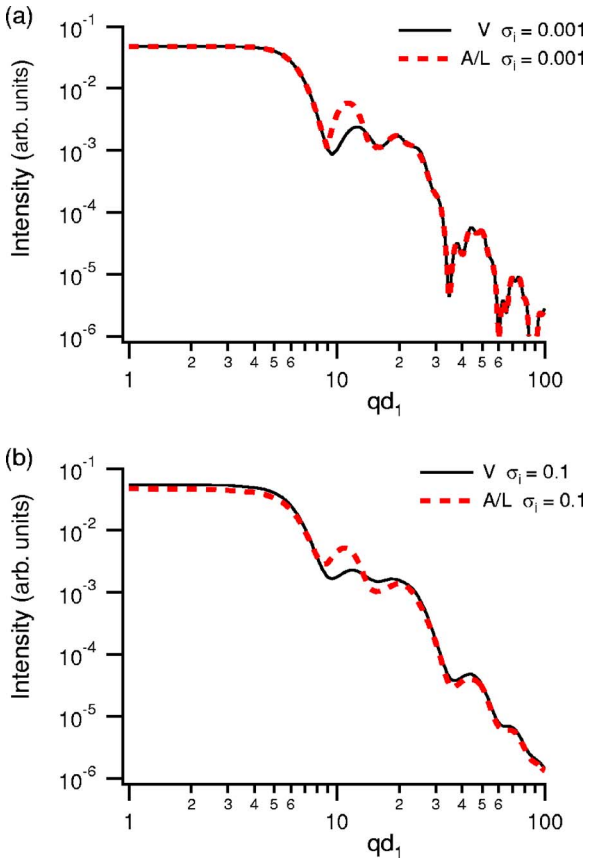

FIG. 2. (Color online) A comparison of the effect of polydispersity on the scattered intensity between the A/L model and the V model for (a) $\sigma_i=0.001$ and (b) $\sigma_i=0.1$ while holding $\varphi_1=\varphi_2=0.2$ and $\alpha=0.25$.

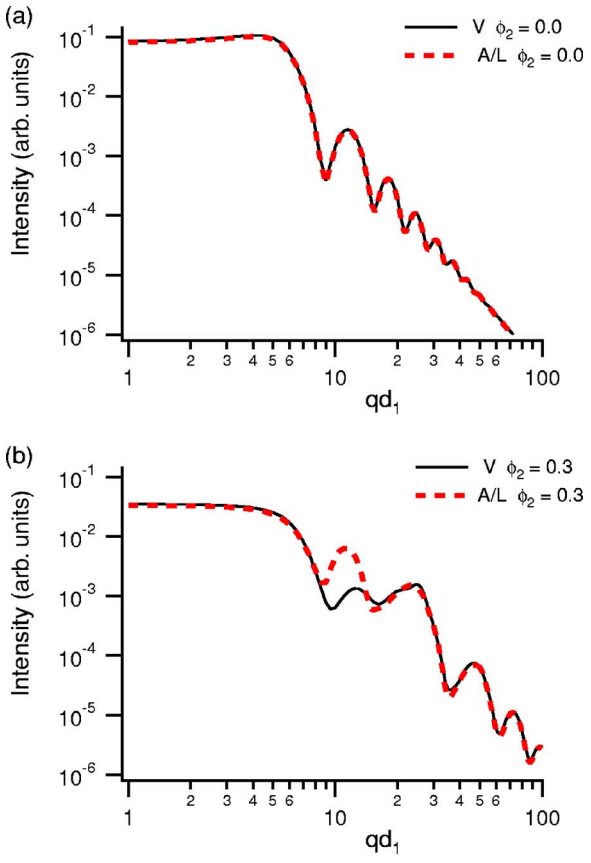

FIG. 3. (Color online) A comparison of the effect of a second component on the scattering intensity between the A/L model and the V model holding $\varphi_1=0.2$, $\sigma_i=0.05$, and $\alpha=0.25$.

$\varphi_1=0.2$ and $\sigma=0.05$. The models predict the same scattering curves for a single component suspension ($\varphi_2=0.0$). As a second smaller component is added to the suspension, the two models predict opposite effects on scattering for intermediate q. In the A/L model, the scattering intensity of the second peak increases, while in the V model, the second peak decreases. The peak also shifts to higher q in the V model. Results from both models rejoin at high q when probing length scales smaller than the size of both particles. Scattering at high q is mostly due to intraparticle scattering accounted for in $P(q)$. It is believed that the difference between the two models lies in the method used to account for interparticle scattering interference summarized by the partial structure factors. In addition, scattering intensity for both models superimpose in the dilute limit ($\varphi_1=\varphi_2\leqslant 0.05$) where the interparticle scattering interference is negligible and intraparticle scattering dominates (results not shown). This observation provides further evidence that these models differ in the way they include interparticle scattering interferences.

III. EXPERIMENT

A. Particle synthesis

Silica particles were synthesized by the base catalyzed hydrolysis and condensation of tetraethylorthosilicate according to the method of Stöber *et al.* [32]. A seeded growth technique originating from Bogush was used to increase particle size [33]. Particles were coated with hydrophobic octadecyl chains through an esterification reaction of surface silanol groups with stearyl alcohol. Once the reaction was completed, excess stearyl alcohol was removed by rinsing with chloroform followed by centrifugation and decantation. Coated particles were dried to ensure the removal of chloroform. Particle sizes of 44±4 nm, 86±5 nm, and 196±9 nm, as determined by scanning electron microscopy (SEM) and transmission electron microscopy (TEM). measurements, were synthesized to make single component suspensions, binary suspensions with size ratios $\alpha=d_2/d_1$ of 0.22 and 0.51, and one ternary suspension with $d_2/d_1=0.51$ and $d_3/d_1=0.22$. Coated particles were suspended in *cis/trans* decalin purchased from Sigma-Aldrich. Single component and binary mixture suspensions were made by weighing out known masses of single component stock suspensions and diluting to the desired volume fraction. Stock suspension volume fractions were determined by dry weights after evaporation of decalin from a known mass of sample using a particle density of 1.8 g/cm^3.

B. USAXS

USAXS was performed at the 33ID-D beam line UNICAT facility located at the Advance Photon Source, Argonne

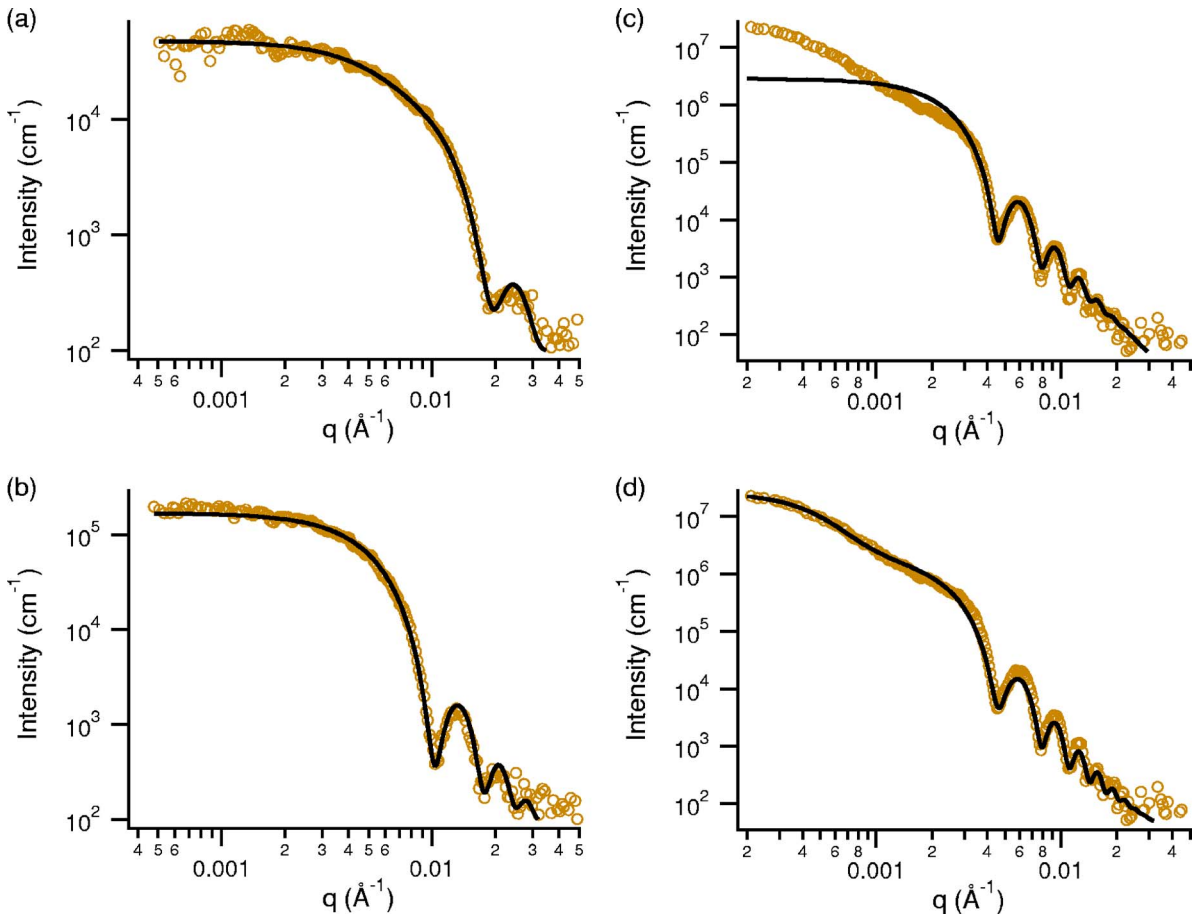

FIG. 4. (Color online) Experimental scattered intensity (○○○) and model fits (solid line) [Eq. (23)] of dilute suspensions (φ_i=0.05) for particle diameters (a) 44 nm, (b) 86 nm, and (c) 196 nm utilizing an average form factor with a single size distribution, and (d) 196 nm with two size distributions.

National Laboratory. The instrument employs a Bonse-Hart camera and a double-crystal Si(111) optics to extend the range of measurements to lower scattering vectors. A pair of horizontally reflecting crystals enabled effective pinhole collimation removing the need for slit desmearing. An absolute calibration converts scattering intensity from counts per second to absolute units of cm^{-1} through knowledge of the sample thickness along the path of the beam. Samples were loaded in custom made aluminum cells. Two kapton polyimide slides sealed the sides of the cell chamber using epoxy perpendicular to the beam path. The beam path length was approximately 1 mm. Measurements on each sample were taken over a period of 30 min. Decalin is considered a nonscatter; therefore, the background intensity was accounted for by measuring scattered intensity of an empty cell enclosed by two kapton polyimide slides. The scattering intensity of the empty cell is subtracted off of the scattering of the sample leaving only scattering due to the silica nanoparticles. The background intensity is dependent on the operation of the instrument and was of the order of 10^2 cm^{-1}.

TABLE I. Particle diameter and standard deviation.

	Size (nm)					
Method	d_1[a]	σ_1[b]	d_2	σ_2	d_3	σ_3
SEM/TEM	196	9	86	5	44	4
Fitting	197	10	87	5	45	4
Guinier	195	N/A	93	N/A	48	N/A

[a] d_i is the particle diameter of particle type i.
[b] σ_i is the standard deviation in the size distribution for particle type i.

C. Hard sphere behavior

Single component suspensions are created in terms of particle volume fraction φ. The scattering intensity [Eq. (1)] in terms of particle volume fraction is written

$$I(q) = \varphi(V_s \Delta\rho_e^2) P(q) S(q).$$

In the dilute limit, the structure factor goes to unity since particle positions are uncorrelated and the scattering is dominated by intraparticle scattering. As a result, the intensity for a dilute suspension is given by

$$I(q) = \varphi(V_s \Delta\rho_e^2) P(q). \quad (23)$$

The degree that the experimental system behaves as hard spheres can be assessed by a comparison of experimental

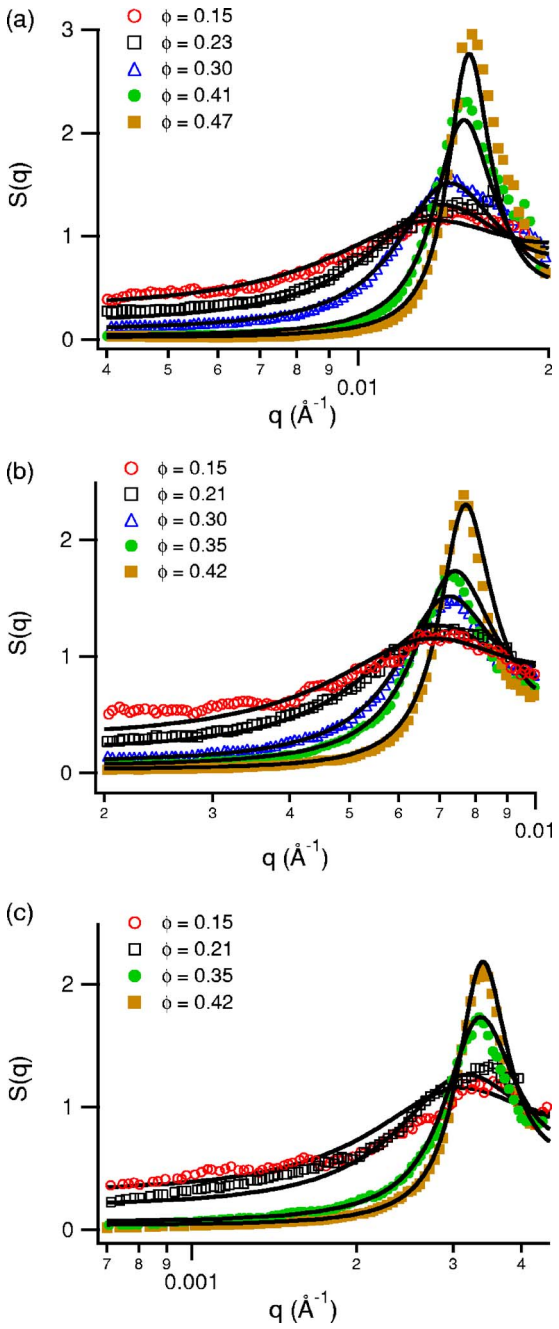

FIG. 5. (Color online) Experimental structure factors are indicated by markers for single component suspensions, (a) 44 nm, (b) 86 nm, and (c) 196 nm, at various volume fractions. Theoretical hard spheres $S(q)$ are drawn through the data points for volume fractions determined from dry weight measurements.

structure factors to theoretical hard sphere structure factors for a monodisperse system. Experimental structure factors for concentrated suspensions (cs) are calculated by dividing the intensity of a concentrated suspension by the intensity of a dilute suspension (ds). The structure factor for the dilute suspension goes to unity leaving $S(q)$ for the concentrated suspension

$$S(q) = \frac{I_{cs}(q,\varphi_{cs})}{I_{ds}(q,\varphi_{ds})}\frac{\varphi_{ds}}{\varphi_{cs}}, \quad \text{typically } \varphi_{ds} \leqslant 0.05. \qquad (24)$$

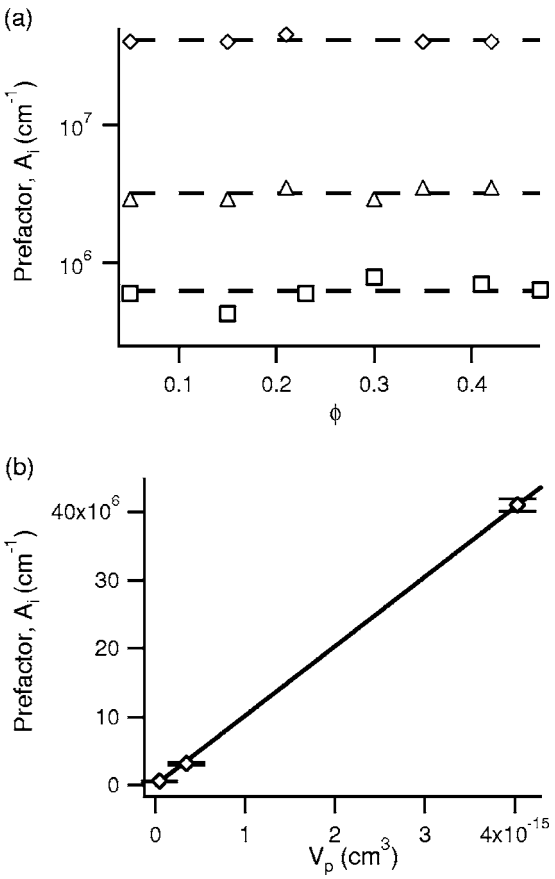

FIG. 6. (a) The scaling prefactors A_i are plotted for single component suspensions with respect to the volume fraction. Dashed lines indicate the mean value. (b) Mean prefactors are plotted with respect to particle volumes. The solid line shows the linear scaling of the prefactor with a particle volume.

D. Electron contrast

While absolute knowledge of the scattering amplitudes are not necessary to determine structure factors for monomodal particle size distributions, as indicated in Eq. (1), absolute scattering from mixtures requires knowledge of f_i. In particular, our application of the Vrij model assumes that electron density contrasts $\Delta\rho_e$ of all particles are the same. We expect the contrast to depend only on the composition and to be independent of particle size. Two methods are used to estimate the contrast. In the first method, the component contrasts are obtained by fitting experimental absolute intensities of single component suspensions to Eq. (24) utilizing

TABLE II. Experimental contrast and standard error.

	Contrast (10^{11} cm^{-2})							
Method	$\Delta\rho_{e,1}$[a]	$s_{e,1}$[b]	$\Delta\rho_{e,2}$	$s_{e,2}$	$\Delta\rho_{e,3}$	$s_{e,3}$	Ave $\Delta\rho_e$	s_e
Fitting	1.0	0.1	1.0	0.1	1.1	0.2	1.03	0.06
Guinier	1.1	N/A	1.1	N/A	1.0	N/A	1.06	0.05

[a] $\Delta\rho_{e,i}$ is the electron density contrast of particles of size i.
[b] $s_{e,i}$ is the standard error in $\Delta\rho_{e,i}$.

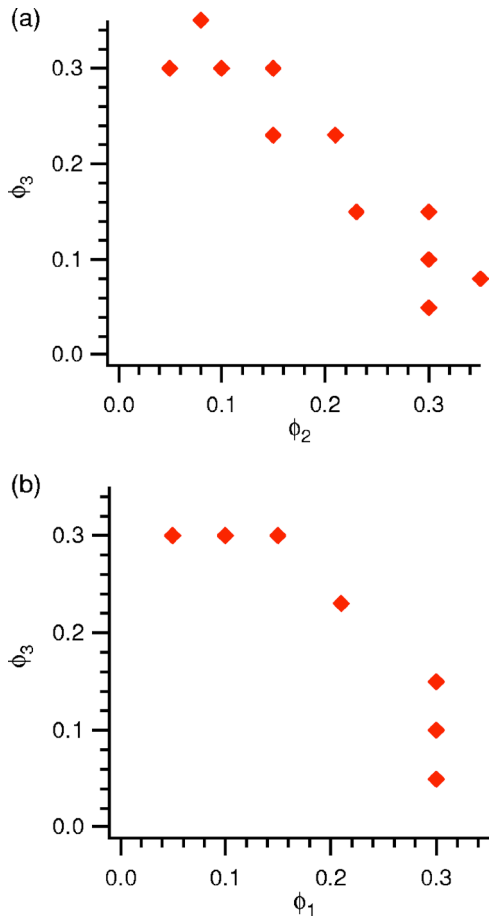

FIG. 7. (Color online) Binary mixtures were made of (a) 44 and 86 nm particles and (b) 44 and 196 nm particles.

Eq. (10) for an average form factor and theoretical hard sphere structure factors calculated in the PY closure. A scattering prefactor, $A_i = V_{s,i}\Delta\rho_e^2$ is calculated from the fitting procedure and is plotted versus particle volume to obtain an average contrast for the silica-decalin suspensions.

In the second method, Guinier's law is used to measure the contrast. Guinier's law requires single particle scattering and is only applicable in the dilute limit where particle positions are uncorrelated. Since the particle positions are uncorrelated, scattering interference between particles is incoherent. Guinier's law applies in the limit $qd_i/2 \leqslant 1$. In this limit, the structure factor goes to unity and the form factor is well approximated by $P(q) = \exp[-q^2 r_g^2/3]$, where r_g is the particle's radius of gyration. A Guinier plot is constructed by plotting the logarithm of $I(q)$ versus q^2:

$$\ln I(q) = \ln(\phi V_s \Delta\rho_e^2) - \frac{q^2 r_g^2}{3}. \tag{25}$$

The contrast is estimated from the intercept as $q \to 0$ and knowledge of the volume fraction and the particle volume. A Guinier plot also provides an estimate of particle size where the radius of gyration is related to a particle diameter by

$$2r_g = d\sqrt{\tfrac{3}{5}}. \tag{26}$$

Guinier radii can be compared to SEM and TEM direct measurements to support contrast estimates.

A third method for determining $\Delta\rho_e$ is to us the method of Porod when in the large q limit, $S(q) \to 1$ and $P(q) \sim 1/q^4$ [34]. In our work, this method was not applied because experimental scattering did not extend into the high q range due to instrumental limitations.

IV. RESULTS

A. Single component suspensions

Scattering from single component suspensions were used to determine mean particle diameters and standard deviations in particle size distributions based on model fits to the form factor and, at higher concentrations, to validate hard sphere behavior by an analysis of the structure factor. Figure 4 displays fits to the scattered intensity for dilute suspensions using average form factors [Eq. (10)]. Experimental scattering is fit to the scattering equation using a least squares regression analysis to minimize the total error by altering fitting parameters: particle size, standard deviation, and the contrast. Particle diameters and standard deviations obtained from fits under dilute conditions are tabulated in Table I.

For the 196 nm particles, model form factors for a monomodel particle size distribution give a poor fit at small scattering angles. We interpret this as arising from the presence of a small number density of aggregates. While the origin of these aggregates is unknown, we believe they form during the synthesis or coating process. These aggregates do not pose a serious threat to the analysis of the mixtures due to their very low number density (i.e., they are always dilute relative to the 196 nm diameter particles). However, these aggregates have a large impact on scattering at low q. The scattering effects of the aggregates can be accounted for by including a second size distribution in the average form factor [Fig. 4(d)]. Assuming that the scattering from the 196 nm diameter particles suspension is composed of 196 nm particles and a second larger size distribution, we estimate that the larger particles are composed of aggregates with a mean diameter of 530 nm with a standard deviation of 360 nm. The relative number density of the aggregates compared to the 196 nm particle is 0.008. Shown in Fig. 4(d) is the form factor fit for a combination of 196 nm diameter particles with a standard deviation of 10 nm in the presence of a dilute population of 530 nm particles with a standard deviation in particle size distribution of 360 nm where the ratio of large to small particle number densities is 0.008.

Structure factors for suspensions containing one particle type are shown in Fig. 5. Here we have extracted an average structure factor using Eq. (25). This process is simplified by using the analytical form factors developed using parameters shown in Table I. The fits to the hard sphere solutions for $S(q)$ are quite satisfactory suggesting interactions between like particles are well approximated by hard core volume exclusion. The discrepancies at low q for the 196 nm particles are attributed to the presence of aggregates in these suspensions. Aggregates blur density fluctuations at length

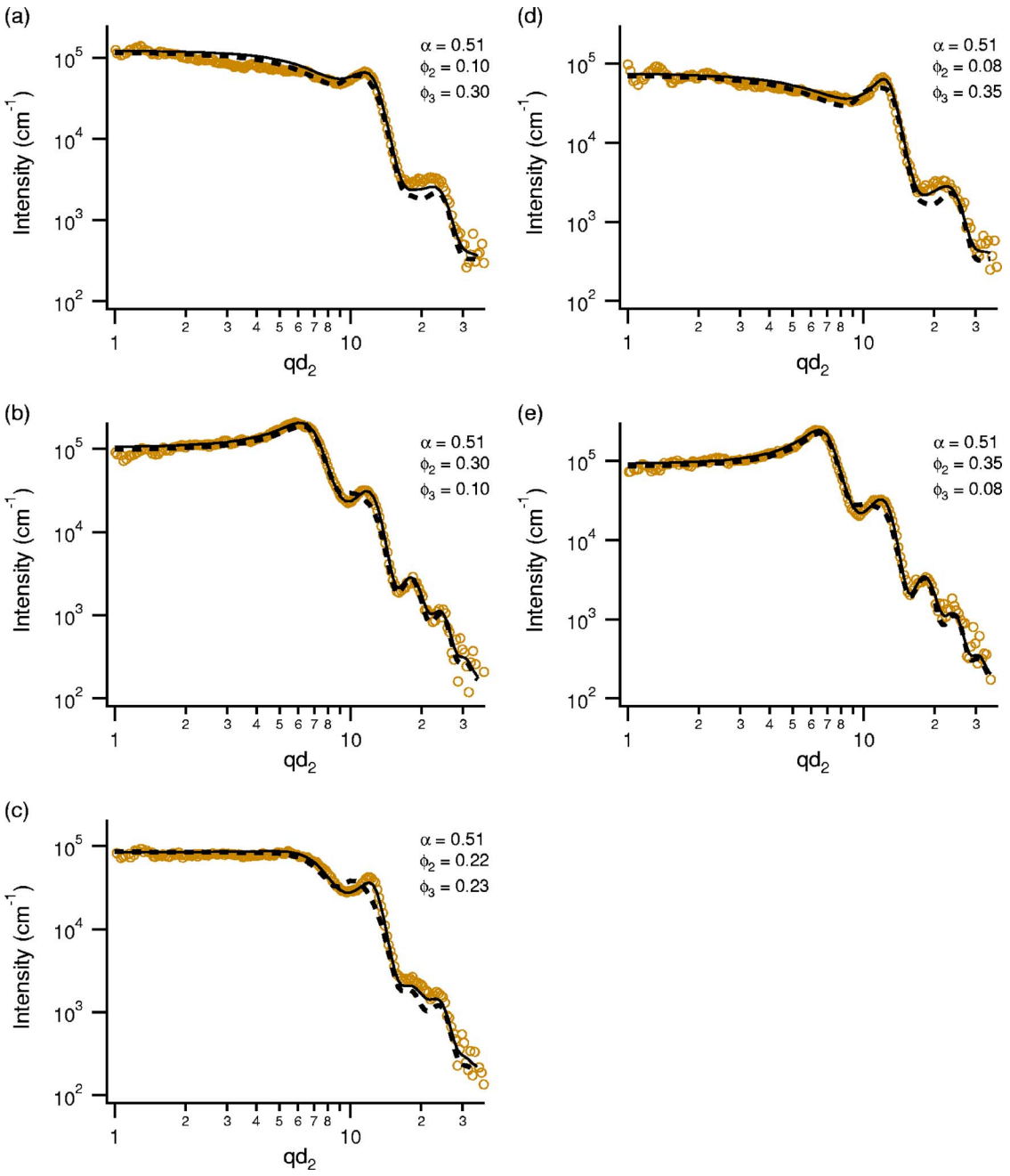

FIG. 8. (Color online) Experimental scattered intensity (○○○) and model fits using the A/L model (dots) and the V model (solid lines) are shown for binary mixtures of 44 and 86 nm particles at indicated volume fractions.

scales larger than the radius of a particle. These effects are manifested in the structure factor at low q.

B. Electron contrasts

The fitting analysis uses a single adjustable parameter to set the magnitude of the total absolute scattering intensity for the single component systems [(i.e. $I_i(q)=A_i\bar{P}_i(q)S_i(q)$, where $\bar{P}_i(q)$ are determined from the best experimental fit at low φ and $S_i(q)$ is determined from the PY solution for single sized particles at the volume fraction of interest]. This technique has the advantage of allowing $\Delta\rho_e$ to be estimated at all volume fractions. The Guinier analysis can only be applied when $S_i(q)=1$ or when $\varphi \leqslant 0.05$. As can be seen in Fig. 6(a), our fitting analysis provides consistent estimates of A_i at all volume fractions for a single particle size distribution. In Fig. 6(b), we show that to within a small uncertainty A_i scales in a linear manner on a particle volume. Contrast estimates from the two analysis methods are tabulated in Table II. The two methods are in agreement within the uncertainty in the measurements.

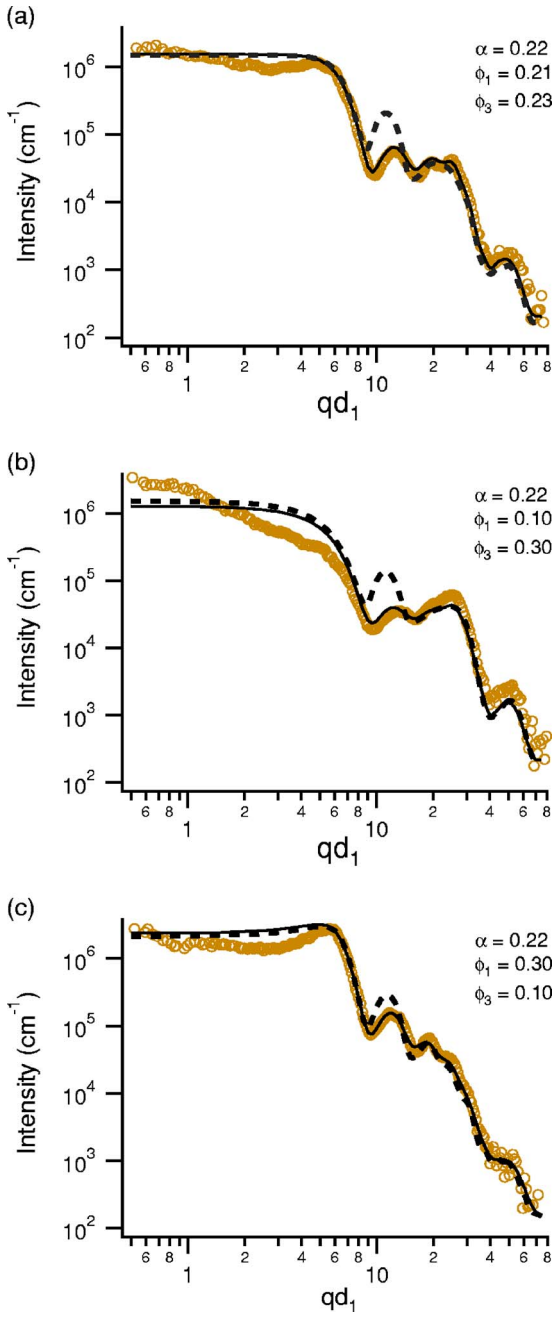

FIG. 9. (Color online) Experimental scattered intensity (○○○) and model fits using the A/L model (dots) and the V model (solid lines) are shown for binary mixtures of 44 and 196 nm particles at indicated volume fractions.

C. Scattering from mixtures

Two component mixtures were made of the 44 and 86 nm particles (α=0.51) and the 44 and 196 nm particles (α =0.22). Volume fractions of the mixtures explored in this study are diagramed in Fig. 7. In Fig. 8, we show scattering intensities as a function of qd_2 and α=0.51 for select volume fraction ratios shown in Fig. 7(a). The significant changes in $I(qd_2)$ at fixed $\varphi=\varphi_2+\varphi_3$ but variable φ_2 are of interest. These changes are seen in comparing Figs. 8(a) and 8(b) and Figs. 8(d) and 8(e). As φ_2 is varied at fixed φ, the positions

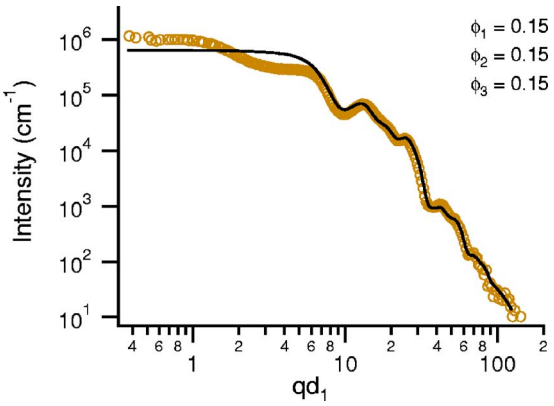

FIG. 10. (Color online) Scattered intensity (○○○) for a ternary mixture of 44, 86 and 196 nm particles is fit using the V model (solid lines) with three size distributions.

and magnitude of maxima shift substantially. The same is true in Fig. 9 where we present scattering from mixtures where α=0.22.

Also shown in Figs. 8 and 9 are predictions of the A/L and V models. As can be seen, the V model more accurately captures both qualitative and quantitative features of the experimental results. This can be attributed to the V model's more accurate account of scattering interferences between particles. The V model's better agreement is seen particularly around the second scattering peak. Discrepancies around the second peak between the A/L model and experiment appear to grow as α is reduced. We believe that we have correctly implemented the A/L model and the V model because our implementation matched results presented in Ashcroft and Langreth [23] and van Buerten and Vrij [29]. We note that the discrepancies found at low q between model and experiment in Fig. 9 are a result of a low volume fraction of poorly characterized aggregates. For these comparisons the particle form factor used for the 196 nm particles does not include the low population density of 530 nm particles. This was done to allow strict comparison of predictions of binary mixture scattering models. One consequence, however, is that we do not anticipate either model to capture the low q scattering of the suspensions of 196 nm particles.

Figure 10 presents the scattering from a ternary mixture of 44, 86, and 196 nm particles with $\varphi_1=\varphi_2=\varphi_3=0.15$ as a function of qd_1, where d_1=196 nm. Again the agreement between predictions of the V model and experiment is astounding for $qd_1>2\pi$. At smaller values of qd_1, the effect of the poorly characterized aggregates becomes important.

In all fits shown in Figs. 8–10, $\bar{P}_i(q)$ and $n(d)$ have been calculated from the data given in Table I. In addition, absolute scattering predictions used electron density contrasts that are within ±10% of the average value shown in Table II. The apparent variation in $\Delta\rho_e$ can easily arise from uncertainties in the sample thickness which is required to convert between detector counts per second to absolute scattering intensity.

The effect of the aggregates on total scattering can be included using the V model for a ternary mixture where we include a third component of d_3=530 nm, σ_3=360 nm, and φ_3=0.01 for a binary mixture with α=0.22, φ_1=0.10, and

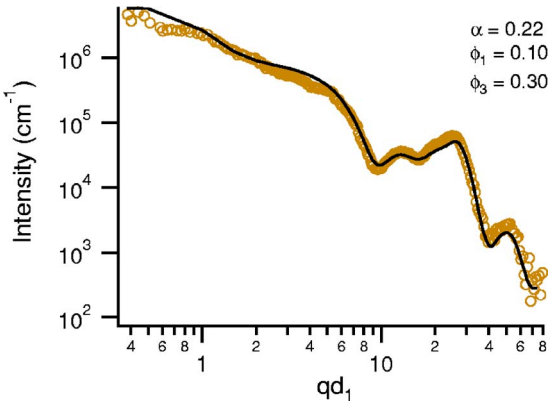

FIG. 11. (Color online) Experimental scattered intensity (○○○) for the binary mixture in 9(b) is fit using the V model (solid lines) with a third size distribution to account for scattering from aggregates of the 196 nm particles.

φ_2=0.30 corresponding to Fig. 9(b). As shown in Fig. 11, this ternary mixture calculation quantitatively captures total scattering intensity over the measurable scattering range.

V. CONCLUSION

The A/L model and V model both capture the qualitative scattering behavior of two component mixtures. The V model was superior to the A/L model for quantitative predictions due to the ease of incorporating the effects of polydispersity in particle size and a more accurate method of calculating interparticle scattering interference. The V model's better accuracy is shown at scattering lengths between the sizes of the two components. The drawback of the V model is that it does not calculate the partial structure factors. The A/L model calculates the partial structure factors; yet, total scattering calculations do not completely match experiment.

The V model is also more practical for data analysis of multicomponent suspensions. It is less computationally intensive than A/L making possible the extension to multicomponent suspensions. The V model uses Baxter's approximation to simplify the direct correlation functions which allows numerical calculations to be easily performed. Additional components are incorporated by adding distributions to the total number density equation. The A/L model is specific to binary systems. An extension to multicomponent systems is difficult due to the complexity of the partial structure factor calculations.

ACKNOWLEDGMENTS

We acknowledge the UNI-CAT facility at the Advanced Photon Source (APS), Argonne National Laboratory where USAXS experiments were performed. The UNI-CAT facility was supported by the U.S. DOE under Grant No. DEFG02-91ER45439, through the Frederick Seitz Materials Research Laboratory at the University of Illinois at Urbana-Champaign, the Oak Ridge National Laboratory (U. S. DOE Contract No. DE-AC05-00OR22725 with UT-Battelle LLC), the National Institute of Standards and Technology (U. S. Department of Commerce), and UOP LLC. The APS is supported by the U.S. DOE, Basic Energy Sciences, Office of Science under Contract No. W-31-109-ENG-38. We also acknowledge the Center for Microanalysis of Materials at the University of Illinois, which is partially supported by the U.S. Department of Energy under Grant No. DEFG02-91-ER45439, where SEM and TEM imaging of particles was performed.

APPENDIX A: A/L MODEL

The coefficients given by Lebowitz [27] are as follows:

$$a_1 = \alpha^{-3}\frac{\partial}{\partial\phi_1}(\beta\rho),$$

$$a_2 = \frac{\partial}{\partial\phi_2}(\beta\rho),$$

$$\beta\rho = \{(\phi_2 + \alpha^3\phi_1)(1 + \phi + \phi^2) - 3\phi_2\phi_1(1-\alpha)^2[1 + \phi_2 + \alpha(1+\phi_1)]\}(1-\phi)^{-3},$$

$$b_1 = -\frac{6}{d_1}\left[\phi_1 g_{11}^2 + \tfrac{1}{4}\phi_2(1+\alpha)^2\alpha^{-3}g_{12}^2\right],$$

$$b_2 = -\frac{6}{d_2}\left[\phi_2 g_{22}^2 + \tfrac{1}{4}\phi_1(1+\alpha)^2\alpha g_{12}^2\right],$$

$$m = \frac{1}{2}\left(\frac{\phi_1 a_1}{d_1^3} + \frac{\phi_2 a_2}{d_2^3}\right).$$

(φ_i is the volume fraction of particle i and $\varphi=\varphi_1+\varphi_2$.)

Radial distribution functions are given by

$$g_{11} = \left[\left(1 + \frac{1}{2}\phi\right) + \frac{3}{2}\phi_2\left(\frac{1}{\alpha} - 1\right)\right](1-\phi)^{-2},$$

$$g_{22} = \left[\left(1 + \frac{1}{2}\phi\right) + \frac{3}{2}\phi_1(\alpha - 1)\right](1-\phi)^{-2},$$

$$g_{12} = \left[\left(1 + \frac{1}{2}\phi\right) + \frac{3}{2}(\phi_2 - \phi_1)\left(\frac{1-\alpha}{1+\alpha}\right)\right](1-\phi)^{-2}.$$

The Fourier transforms of the direct correlation functions as given by Ashcroft and Langreth [23] are

$$-n_1C_{11}(q)=\frac{24\phi_1}{q^3d_1^3}\Bigg\{a_1\sin qd_1-qd_1\cos qd_1+\frac{b_1}{q}[2qd_1\sin qd_1-(q^2d_1^2-2)\cos qd_1-2]+\frac{d_1m}{q^2}[(4q^2d_1^2-24)\sin qd_1$$
$$-(q^4d_1^4-12q^2d_1^2+24)\cos qd_1+24]\Bigg\}, \tag{A1}$$

$$-n_2C_{22}(q)=\text{same as}-n_1C_{11}(q)\ \text{but replace}\ \phi_1\rightarrow\phi_2,d_1\rightarrow d_2,a_1\rightarrow a_2,b_1\rightarrow b_2, \tag{A2}$$

$$-n_1^{1/2}n_2^{1/2}C_{12}(q)=3(1-\alpha)^3\frac{\phi x_1^{1/2}x_2^{1/2}}{x_1+x_2\alpha^3}a_2\frac{\sin y_q-y_q\cos y_q}{y_q^3}+24\phi\frac{x_1^{1/2}x_2^{1/2}\alpha^3}{x_1+x_2\alpha^3}\Bigg[\frac{\sin y_q}{q^4d_2^4}\Bigg\{\beta_{12}[2qd_2\cos qd_2+(q^2d_2^2-2)\sin qd_2]$$
$$+\frac{\gamma_{12}}{qd_2}[(3q^2d_2^2-6)\cos qd_2+(q^3d_2^3-6qd_2)\sin qd_2+6]+\frac{d_2m}{q^2}[(4q^3d_2^3-24qd_2)\cos qd_2+(q^4d_2^4$$
$$-12q^2d_2^2+24)\sin qd_2]\Bigg\}+\frac{\cos y_q}{q^4d_2^4}\Bigg\{\beta_{12}[2qd_2\sin qd_2-(q^2d_2^2-2)\cos qd_2-2]+\frac{\gamma_{12}}{qd_2}[(3q^2d_2^2-6)\sin qd_2$$
$$-(q^3d_2^3-6qd_2)\cos qd_2]+\frac{d_2m}{q^2}[(4q^3d_2^3-24qd_2)\sin qd_2-(q^4d_2^4-12q^2d_2^2+24)\cos qd_2+24]\Bigg\}$$
$$+\frac{a_2}{qd_2}\Bigg\{\cos y_q\left(\frac{\sin qd_2-\mathrm{qd}_2\cos qd_2}{q^2d_2^2}+\frac{(1-\alpha)}{2\alpha}\frac{(1-\cos qd_2)}{qd_2}\right)+\sin y_q\left(\frac{\cos qd_2-qd_2\sin qd_2-1}{q^2d_2^2}$$
$$+\frac{(1-\alpha)}{2\alpha}\frac{(\sin qd_2)}{qd_2}\right)\Bigg\}\Bigg], \tag{A3}$$

where $x_1=n_1/n$, $x_2=n_2/n$, $y_q=\frac{1}{2}q(d_1-d_2)$, $\gamma_{12}=2md_2^2(d_1-d_2)$, and

$$\beta_{12}=-3d_2(d_1+d_2)\left(\frac{\phi_1g_{11}}{d_1^2}+\frac{\phi_2g_{22}}{d_2^2}\right)g_{12}.$$

APPENDIX B: V MODEL

Expressions for the terms $\Delta(q)$ and $D_f(q)$ are given below. The interested reader should consult Vrij [25] for a detailed derivation of the expressions.

$$\Delta(q)=(1-\xi_3)^{-4}[(F_{11}F_{22}-F_{12}^*F_{21}^*)(F_{11}^*F_{22}^*-F_{12}^*F_{21}^*)], \tag{B1}$$

where

$$F_{11}(q)=1-\xi_3+\langle d^3e^{\mathrm{iX}}\Phi\rangle,$$

$$F_{12}(q)=\langle d^4e^{\mathrm{iX}}\Phi\rangle,$$

$$F_{22}(q)=1-\xi_3+3\langle d^3e^{\mathrm{iX}}\Psi\rangle,$$

$$F_{21}(q)=\tfrac{1}{2}(1-\xi_3)iq-3\xi_2+3\langle d^2e^{\mathrm{iX}}\Psi\rangle.$$

$F_{\alpha\beta}^*$ is the complex conjugate of $F_{\alpha\beta}$.

The determinant $D_f(q)$ is

$$D_f(q)=-\left(\frac{6}{\pi}\right)(1-\xi_3)^{-4}[\langle f^2B^2\rangle T_1T_1^*+\langle d^6\Phi^2\rangle T_2T_2^*$$
$$+9\langle d^4\Psi^2\rangle T_3T_3^*+\langle fB\,d^3\Phi\rangle(T_1T_2^*+T_1^*T_2)+3\langle fB\,d^2\Psi\rangle$$
$$\times(T_1T_3^*+T_1^*T_3)+3\langle d^5\Phi\Psi\rangle(T_2T_3^*+T_2^*T_3)], \tag{B2}$$

where

$$T_1=F_{11}F_{22}-F_{12}F_{21},$$

$$T_2=F_{21}\langle df\,Be^{\mathrm{iX}}\rangle-F_{22}\langle fBe^{\mathrm{iX}}\rangle,$$

$$T_3=F_{12}\langle fBe^{\mathrm{iX}}\rangle-F_{11}\langle df\,Be^{\mathrm{iX}}\rangle.$$

Expressions for additional terms are

$$X_\mathrm{i}=\tfrac{1}{2}qd_\mathrm{ii},$$

$$\Psi(X_\mathrm{i})=X_\mathrm{i}^{-1}\sin X_\mathrm{i},$$

$$\Phi(\mathrm{X_i})=3X_\mathrm{i}^{-3}(\sin X_\mathrm{i}-X_\mathrm{i}\cos X_\mathrm{i}),$$

$$B_\mathrm{i}=P_\mathrm{i}(q)^{1/2}=3\frac{\sin(qd_\mathrm{ii}/2)-(qd_\mathrm{ii}/2)\cos(qd_\mathrm{ii}/2)}{(qd_\mathrm{ii}/2)^3},$$

and $f_\mathrm{i}=d_\mathrm{ii}^3\Delta\rho_\mathrm{e}$.

Brackets $\langle\ \rangle$ denote an average performed over all components of the mixture:

$$\langle f^2B^2\rangle=\left(\frac{\pi}{6}\right)\sum_{\mathrm{i}=1}^{p}n_\mathrm{i}f_\mathrm{i}^2B_\mathrm{i}^2.$$

[1] M. K. Chow and C. F. Zukoski, J. Rheol. **39**, 15 (1995).
[2] J. Bender and N. J. Wagner, J. Rheol. **40**, 899 (1996).
[3] P. N. Pusey and W. van Megen, Phys. Rev. Lett. **59**, 2083 (1987).
[4] L. Marshall and C. F. Zukoski, J. Phys. Chem. **94**, 1164 (1990).
[5] W. van Megen and S. M. Underwood, Phys. Rev. E **49**, 4206 (1994).
[6] R. J. Phillips, J. F. Brady, and G. Bossis, Phys. Fluids **31**, 3462 (1988).
[7] P. N. Segre, O. P. Behrend, and P. N. Pusey, Phys. Rev. E **52**, 5070 (1995).
[8] E. G. D. Cohen, R. Verberg, and I. M. de Schepper, Physica A **251**, 251 (1998).
[9] S. A. Shah, Y.-L Chen, K. S. Schweizer, and C. F. Zukoski, J. Chem. Phys. **118**, 3350 (2003).
[10] S. A. Shah, Y. L. Chen, S. Ramakrishnan, K. S. Schweizer, and C. F. Zukoski, J. Phys. I **15**, 4751 (2003).
[11] P. G. Bolhuis, A. A. Louis, and J. P. Hansen, Phys. Rev. Lett. **89**, 128302 (2002).
[12] S. Ramakrishnan, M. Fuchs, K. S. Schweizer, and C. F. Zukoski, J. Chem. Phys. **116**, 2201 (2002).
[13] M. Fuch and K. S. Schweizer, Europhys. Lett. **51**, 621 (2000).
[14] M. Dijkstra, J. M. Brader, and R. Evans, J. Phys.: Condens. Matter **11**, 10 079 (1999).
[15] M. H. G. Duits, R. P. May, A. Vrij, and C. G. de Kruif, J. Chem. Phys. **94**, 4521 (1991).
[16] B. E. Rodriguez and E. W. Kaler, Langmuir **8**, 2376 (1992).
[17] J. M. Mendez-Alcaraz, B. D'Aguanno, and R. Klein, Langmuir **8**, 2913 (1992).
[18] R. H. Ottewill, A. R Rennie, and G. D. W. Johnson, Adv. Colloid Interface Sci. **100**, 585 (2003).
[19] S. R. Williams and W. van Megen, Phys. Rev. E **64**, 041502 (2001).
[20] W. J. Hunt and C. F. Zukoski, Langmuir **12**, 6257 (1996).
[21] W. J. Hunt and C. F. Zukoski, J. Colloid Interface Sci. **210**, 332 (1999).
[22] B. E. Rodriguez, E. W. Kaler, and M. S. Wolfe, Langmuir **8**, 2382 (1992).
[23] A. T. J. M. Woutersen and C. G. de Kruif, J. Rheol. **37**, 681 (1993).
[24] N. J. Wagner and A. T. J. M. Woutersen, J. Fluid Mech. **278**, 267 (1994).
[25] N. W. Ashcroft and D. C. Langreth, Phys. Rev. **156**, 685 (1967).
[26] A. König and N. W. Ashcroft, Phys. Rev. E **63**, 041203 (2001).
[27] L. Blum and G. Stell, J. Chem. Phys. **71**, 42 (1979).
[28] A. Vrij, J. Chem. Phys. **71**, 3267 (1979).
[29] P. van Buerten and A. Vrij, J. Chem. Phys. **74**, 2744 (1981).
[30] J. L. Lebowitz, Phys. Rev. **133**, A895 (1964).
[31] R. J. Baxter, J. Chem. Phys. **52**, 4559 (1970).
[32] W. Stöber, A. Fink, and E. Bohn, J. Colloid Interface Sci. **26**, 62 (1968).
[33] G. H. Bogush, M. A. Tracy, and C. F. Zukoski, J. Non-Cryst. Solids **104**, 95 (1988).
[34] R. Roe, *Methods of x-ray and Neutron Scattering in Polymer Science*, (Oxford University Press, New York, 2000) p. 178.